ADVANCED MATERIALS
www.advmat.de

Boosting Catalysis of Pd Nanoparticles in MOFs by Pore Wall Engineering: The Roles of Electron Transfer and Adsorption Energy

*Dongxiao Chen, Weijie Yang, Long Jiao, Luyan Li, Shu-Hong Yu, and Hai-Long Jiang**

The chemical environment of metal nanoparticles (NPs) possesses significant influence on their catalytic performance yet is far from being well understood. Herein, tiny Pd NPs are encapsulated into the pore space of metal–organic frameworks (MOFs), UiO-66-X (X = H, OMe, NH_2, 2OH, 2OH(Hf)), affording Pd@UiO-66-X composites. The surface microenvironment of the Pd NPs is readily modulated by pore wall engineering, via the functional group and metal substitution in the MOFs. Consequently, the catalytic activity of Pd@UiO-66-X follows the order of Pd@UiO-66-OH > Pd@UiO-66-2OH(Hf) > Pd@UiO-66-NH_2 > Pd@UiO-66-OMe > Pd@UiO-66-H toward the hydrogenation of benzoic acid. It is found that the activity difference is not only ascribed to the distinct charge transfer between Pd and the MOF, but is also explained by the discriminated substrate adsorption energy of Pd@UiO-66-X (–OH < –2OH(Hf) < –NH_2 < –OMe < –H), based on CO-diffuse reflectance infrared Fourier transform spectra and density-functional theory (DFT) calculations. The Pd@UiO-66-OH, featuring a high Pd electronic state and moderate adsorption energy, displays the highest activity. This work highlights the influence of the surface microenvironment of guest metal NPs, the catalytic activity of which is dominated by electron transfer and the adsorption energy, via the systematic substitution of metal and functional groups in host MOFs.

Catalysis has greatly promoted the progress of human life and industrial production, where the catalyst plays the key role. Metal nanoparticles (NPs) as an important class of heterogeneous catalysts have been widely used in various reactions; for example, Pd NPs are most commonly used in hydrogenation reactions because of their high activity.[1] However, small metal NPs are prone to aggregate during the reaction due to their high surface energy, and their catalytic activity is severely influenced by surrounding chemical environment. To address the above issues, there are two common solutions: (1) protecting metal NPs with various ligands or surfactants, where the accessibility of metal sites is usually hampered by these surface protectors; (2) stabilizing metal NPs onto supports, where the interface interaction between the support and metal NPs is limited, thus causing stability and selectivity concerns. In fact, the surface microenvironment modulation of metal NPs based on conventional supports, such as metal oxides, is far from satisfaction and difficult to achieve.[2] In this context, encapsulating metal NPs into porous materials has been recently recognized to be an effective strategy,[2a–c] where the hosts are able to stabilize metal NPs in small sizes and make them well accessible to the substrates thanks to the interconnected pores. The substrate can be even enriched inside the nanoreactor via capillary action, accelerating the catalysis. Moreover, it is possible to regulate the microenvironment around metal active sites via pore wall engineering of the porous hosts.

To meet this target, metal–organic frameworks (MOFs), a class of crystalline porous materials featuring well-tailorable linkers, clusters and pore spaces,[3] would be ideal host materials. MOFs with permanent porosity offer inherent advantages to confine metal NPs and the resultant metal NPs@MOF composites have demonstrated their great potential and integrated merits of both components for enhanced catalysis.[4] In recent years, there have been quite a few reports on metal NPs@MOF catalysis, most of which concern about the high activity and recyclability of tiny metal NPs stabilized by MOF hosts.[4] In fact, the chemical microenvironment around guest metal NPs can be easily regulated, by the linker functional group alteration or metal substitution in MOFs, to improve the activity.[2c,5] However, the current limited investigations are almost related to linker or metal alteration only,[5] and the microenvironment influence figure of metal NPs for catalysis remains largely unclear. To the best of our knowledge, there has never been a report on the systematic interaction regulation between guest

D. Chen, Dr. L. Jiao, L. Li, Prof. S.-H. Yu, Prof. H.-L. Jiang
Hefei National Laboratory for Physical Sciences at the Microscale
CAS Key Laboratory of Soft Matter Chemistry
Collaborative Innovation Center of Suzhou Nano Science and Technology
Department of Chemistry
University of Science and Technology of China
Hefei, Anhui 230026, P. R. China
E-mail: jianglab@ustc.edu.cn
Dr. W. Yang
School of Energy and Power Engineering
North China Electric Power University
Baoding, Hebei 071003, P.R. China
The ORCID identification number(s) for the author(s) of this article can be found under https://doi.org/10.1002/adma.202000041.

DOI: 10.1002/adma.202000041

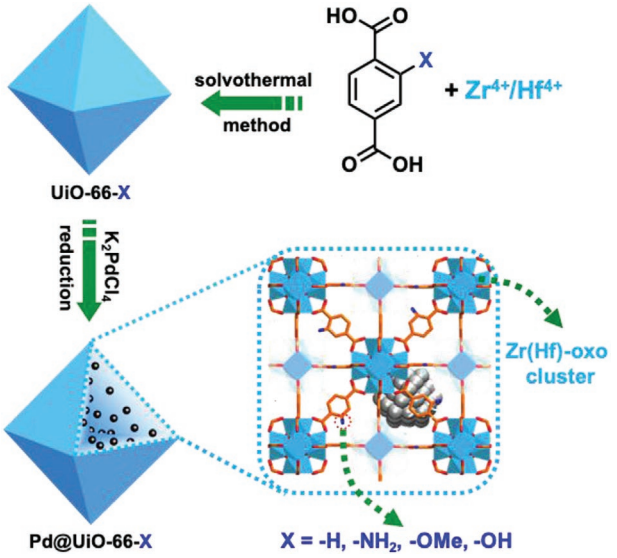

Scheme 1. Schematic illustration showing the preparation process of Pd@UiO-66-X and highlighting their tailorable pore walls.

metal NPs and host MOFs by changing both linker and metal clusters for catalysis.

In this work, isoreticular MOFs with the UiO-66 structural prototype featuring alterable linker groups and metal clusters[6] are employed to encapsulate Pd NPs via the ultrasound-assisted double-solvent approach (DSA),[7] affording Pd@UiO-66-X (X = H, OMe, NH_2, 2OH, 2OH(Hf); X represents the alterable group grafting onto the linker benzene ring, Hf means the Hf-oxo or otherwise the Zr-oxo cluster; Scheme 1). The obtained Pd@UiO-66-X exhibits distinctly different activities in the hydrogenation reaction of benzoic acid, in which Pd@UiO-66-2OH possesses the highest activity followed by Pd@UiO-66-2OH(Hf), Pd@UiO-66-NH_2, Pd@UiO-66-OMe, and Pd@UiO-66, in a decreasing order of activity. Remarkably, the activity of Pd@UiO-66-2OH is around 14 times higher than that of Pd@UiO-66. The distinct activity is not only ascribed to the different electron transfer from Pd to the MOFs, but also due to the discriminated substrate adsorption energy of Pd@UiO-66-X, as elucidated by density-functional theory (DFT) calculations. This is the first finding that electron transfer and substrate adsorption energy codominate the activity in metal NPs/MOF catalytic system.

The UiO-66-X frameworks, formulated $M_6O_4(OH)_4(BDC\text{-}X)_6$ (BDC = benzene-1,4-dicarboxylate; M = Zr, X = H, NH_2, OMe, 2OH; M = Hf, X = 2OH),[6] as the representative MOFs, was employed as hosts. UiO-66-X features a 3D network with two types of cages with diameters of 0.8 and 1.1 nm, high physicochemical stability, suitable for stabilizing tiny metal NPs. The five isoreticular UiO-66-X with pore sizes of 7–12 Å have been synthesized according to the previous methods with slight modifications (Scheme 1).[6] To prevent the formation of Pd NPs on the MOF external surface, avoid Pd aggregation and achieve sufficient contact between Pd and the MOF, an ultrasound assisted DSA[7] was adopted to rationally incorporate Pd NPs to afford Pd@UiO-66-X (Scheme 1; also see experimental details in the Supporting Information).

The phase purity and crystallinity of all UiO-66-X and Pd@UiO-66-X have been examined by powder X-ray diffraction (XRD, Figure S1, Supporting Information). All Pd@UiO-66-X well inherit the structure from UiO-66 while do not show any diffraction peak for Pd NPs, revealing that Pd NPs could be small. The Brunauer–Emmett–Teller (BET) surface area and pore size distribution of Pd@UiO-66-X have been investigated by nitrogen sorption at 77 K (Figures S2 and S3 and Table S1, Supporting Information). The decreased surface area upon introducing different functional groups is caused by the partial pore occupation of functional groups in MOFs. In reference to the parent UiO-66-X, the slight decreased surface of Pd@UiO-66-X is possibly due to the occupied pore space and increased weight by Pd NPs.[7b] Meanwhile, all Pd@UiO-66-X catalysts show similar pore size distributions, making them ideal candidates to investigate the influence of chemical environment exclusively (Figure S3b, Supporting Information). Transmission electron microscopy (TEM) observation for Pd@UiO-66-NH_2 as a representative suggests that very tiny Pd NPs are highly dispersed with mean sizes less than 1.1 nm throughout the entire MOF particle (**Figure 1**a,b; Figures S4–S7, Supporting Information). This is further approved by the elemental energy-dispersive X-ray (EDX) mapping (Figure 1c). It is reasonably considered that most of Pd NPs with sizes similar to or less than the diameter of the MOF cages are successfully confined in the MOF as predesigned. The inductively coupled plasma atomic emission spectroscopy (ICP-AES) results reveal that the Pd contents in Pd@UiO-66-X are similar and fall in the range of 2.13–2.84 wt % (Table S1, Supporting Information).

Upon demonstrating the similar structure and components of Pd@UiO-66-X, we set out to explore their catalytic performance toward hydrogenation of benzoic acid (**Table 1**). The selective

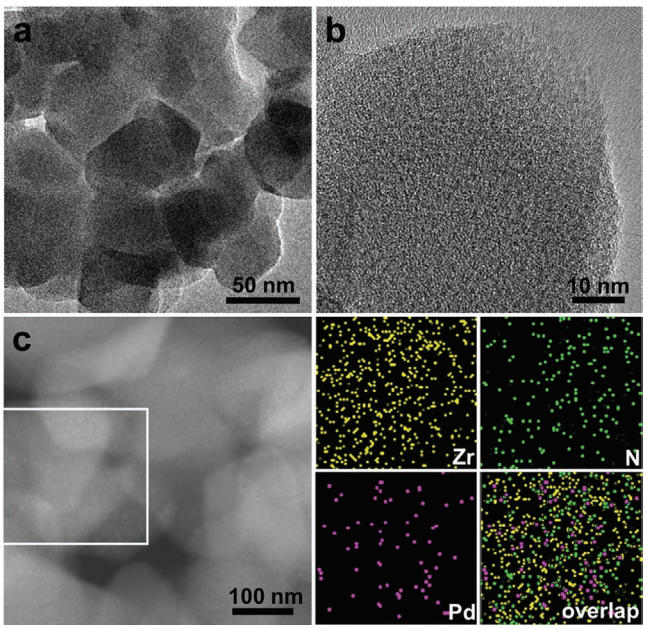

Figure 1. a,b) Representative low-magnification (a) and high-magnification (b) TEM images of Pd@UiO-66-NH_2. c) High-angle annular dark-field scanning transmission electron microscopy (HAADF-STEM) image of Pd@UiO-66-NH_2, and the corresponding Zr, N, Pd, and overlapped elemental mapping for the selected area.

Table 1. The preliminary optimization experiments for the hydrogenation of benzoic acid.

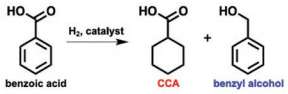

Entry[a)]	Catalyst	H_2 Pressure [bar]	Temperature [°C]	Solvent	Conv.	Sel.
1	no	10	85	water	0%	—
2	UiO-66-2OH	10	85	water	0%	—
3	Pd@UiO-66-2OH	10	85	water	>99%	100%
4	Pd@UiO-66-2OH	1	85	water	12%	100%
5	Pd@UiO-66-2OH	10	50	water	6%	100%
6	Pd@UiO-66-2OH	10	85	DMF	0%	—
7	Pd@UiO-66-2OH	10	85	dioxane	0%	—

[a)]Reaction conditions: 0.1 mmol benzoic acid, 5 mL solvent, 15 mg catalyst, 8 h at different temperatures or H_2 pressures. Catalytic products were analyzed and identified by gas chromatography.

hydrogenation of benzoic acid to cyclohexanecarboxylic acid (CCA) not only affords highly desired chemical intermediate for the synthesis of pharmaceuticals such as praziquantel, but also is a significant process in the synthesis of caprolactam from toluene.[8] The preliminary optimization experiments have been conducted to obtain optimized reaction conditions (Table 1). No product can be detected in the absence of catalyst or in the presence of pure MOF catalyst only (entry 1–2). In sharp contrast, Pd@UiO-66-2OH gives complete conversion under the identical conditions (in water at 85 °C and 10 bar, entry 3), which unambiguously indicates that Pd NPs behave as the catalytic centers for this process. Interestingly, the conversion quickly decreases when the reaction pressure or temperature goes down (entry 4–5). It is delighted to find that the most favorable green solvent, water, is optimal for this reaction; no product is surprisingly detectable in DMF and dioxane (entry 6–7).

With the above optimized reaction parameters, the Pd@UiO-66-X with different functional groups and metal clusters, in a fixed amount, have been attempted for the selective hydrogenation of benzoic acid. Strikingly, they show distinctly different catalytic activity, although they have similar components and structures. The Pd@UiO-66-2OH affords nearly complete conversion (>99%) in 8 h and the reaction proceeds efficiently in the first order rate (**Figure 2**a). By contrast, Pd@UiO-66-NH_2, Pd@UiO-66-OMe, and Pd@UiO-66 give gradually decreased conversions of 73%, 30%, and 7%, respectively, under the same conditions (Figure 2b). Interestingly, upon changing the Zr-oxo to Hf-oxo cluster, the resulting Pd@UiO-66-2OH(Hf) exhibits moderate activity with a conversion of 79%. To our delight, all these catalysts are able to convert benzoic acid to CCA product with complete selectivity (Figure 2b). More importantly, no apparent loss of MOF crystallinity and no identifiable peak for Pd NPs are observed in the powder XRD pattern after catalysis (Figure S8, Supporting Information). The results suggest the retained integrity of UiO-66-2OH framework and the absence of Pd agglomeration, which is

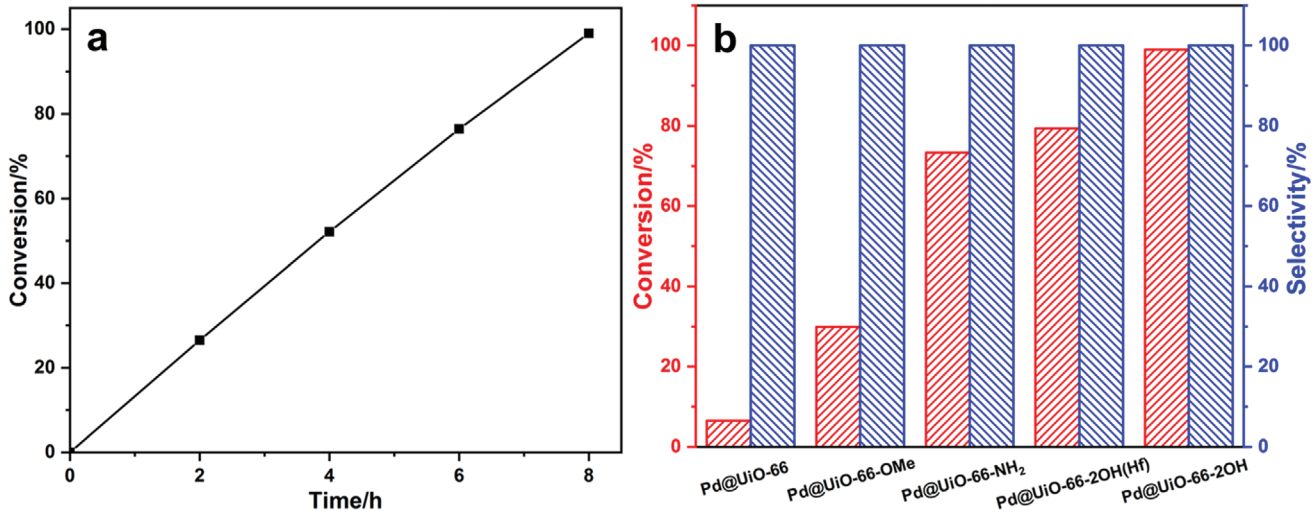

Figure 2. a) Time-dependent conversion of selective benzoic acid hydrogenation over Pd@UiO-66-2OH. b) Conversion and selectivity of catalytic hydrogenation of benzoic acid over Pd@UiO-66-X. Reaction conditions: 0.1 mmol BA, 5 mL water, 15 mg catalyst, 8 h, 85 °C, 10 bar H_2.

further approved by the TEM observation (Figure S9, Supporting Information), demonstrating the great MOF confinement effect and structural stability of the composite catalysts. In addition, the durability of Pd@UiO-66-2OH has been further examined with the reaction carried out by using three times larger amount of benzoic acid. As expected, no apparent activity drop of Pd@UiO-66-2OH can be observed during the reaction; the reaction proceeds efficiently and reaches complete conversion within 22 h (Figure S10, Supporting Information). To verify the nature of the heterogeneous catalysis of Pd@UiO-66-2OH, the filtration test has been performed. It can be seen that no further conversion of benzoic acid can be detected upon the removal of the catalyst, reflecting the heterogeneous feature of the catalytic process (Figure S11, Supporting Information). Furthermore, only a tiny amount of Pd leaching (≈3.9%) is observed from the catalyst after reaction and the activity of Pd@UiO-66-2OH shows very slight drop in the three consecutive cycles (Figure S12, Supporting Information).

Although water possibly participates in the hydrogenation reaction by providing proton as the reductant,[8b] it is safe to conclude that such effect from water would not contribute to the catalytic differences in our work, as all reactions have been carried out under the same conditions. It is assumed that surface electronic properties of confined Pd NPs are responsible for the activity difference. To understand the real reason behind this significant activity difference among Pd@UiO-66-X and elucidate the corresponding Pd surface electronic states, DFT calculations have been adopted to obtain the Bader charge and *d*-band center of these composite catalysts, using the Vienna Ab initio Simulation Package (VASP) with plane-wave pseudo potential method.[9] On the basis of the optimized geometries of Pd_{28}@UiO-66-X, the numbers of electron transfer from Pd clusters to the host frameworks in UiO-66-2OH, UiO-66-2OH(Hf), UiO-66-NH_2, UiO-66-OMe, and UiO-66, featuring fixed framework topology yet altered functional groups on the BDC linker or exchanged metals in the M-oxo cluster, are 2.62, 2.57, 2.63, 2.68, and 2.89, respectively (**Figure 3**a). As expected, such a trend is well consistent with the activity sequence for all the UiO-66-X structures with Zr-oxo clusters, implying that the charge transfer between Pd and the MOFs is responsible for their discriminated activities. On the basis of the electron density distribution profile, it is obvious that electron transfer mainly takes place at the region between Pd NPs and linkers. To be specific, the accumulation of electron density is mostly located at the bond of Pd and linkers, whereas the reduction of electron density is mostly located at Pd NPs and linkers (Figure 3a inset; Figure S13, Supporting Information), indicating that the MOFs are able to hold Pd NPs firmly. Meanwhile, the Pd NPs lose electrons, presenting positive charge, which is in consistent with the analysis of Bader charge.

To further understand the above different electron transfer numbers and probe into the surface electron property of Pd NPs encapsulated in UiO-66-X, the diffuse reflectance infrared Fourier transform (DRIFT) spectra of CO adsorption has been carried out to evaluate the adsorption behavior of CO molecule on the Pd NPs (Figure 3b). The main adsorption peaks of all five samples falls into the range of 2020–2075 cm^{-1}, which are assigned to the C–O vibrations of linearly adsorbed CO. The adsorption mode of CO of all five samples is the same which suggests that Pd NPs in these sample are of the same structure and situation. No bridge-bonded peaks (1850–1950 cm^{-1}) are observable from the spectra. The small peaks around 2121 cm^{-1} are possibly due to CO adsorbed on the partially oxidized Pd NPs.[10] The main adsorption peaks of all five samples exhibit apparent redshift, assignable to the electron-donating effect of functional groups on the linkers in the host MOFs to the guest Pd NPs. The electron donation degree follows the order of

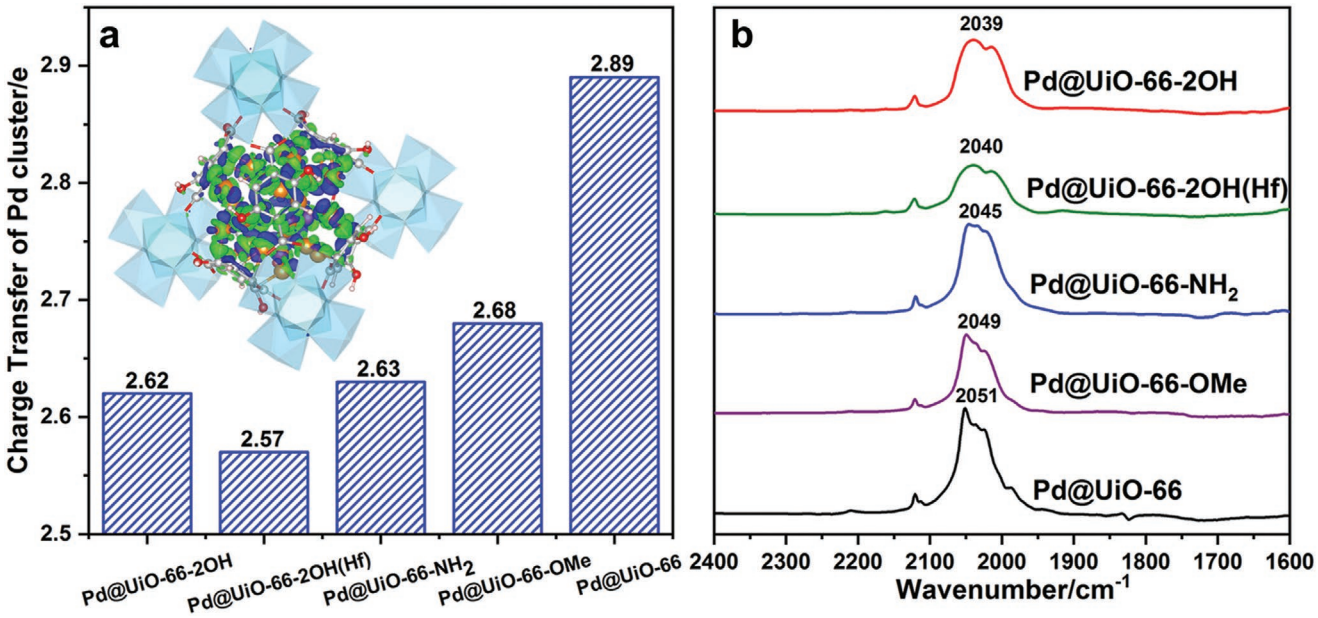

Figure 3. a) The calculated number of electron transfer from Pd clusters to the MOF host in Pd@UiO-66-X (inset: electron density distribution profile of Pd@UiO-66-2OH as a representative). b) The DRIFT spectra of CO adsorption on Pd@UiO-66-X at 298 K.

Pd@UiO-66-2OH > Pd@UiO-66-2OH(Hf) > Pd@UiO-66-NH_2 > Pd@UiO-66-OMe > Pd@UiO-66, which provides perfect explanation (i.e., charge compensation from the functional groups to Pd NPs) on the reversed order of electron transfer numbers in the above calculated results.

In addition, the position of the center of the *d*-band states (ε_d) of Pd NPs (using Pd_{28} as a representative structural model) encapsulated in different UiO-66-X frameworks was calculated as follows

$$\varepsilon_d = \frac{\int_{-\infty}^{+\infty} E \cdot D(E)\,dE}{\int_{-\infty}^{+\infty} D(E)\,dE} \quad (1)$$

where $D(E)$ is the density of d-states function of the Pd atoms and E is the energy relative to the Fermi level.

According to the theory of *d*-band center,[9,11] a higher *d*-band center location (less electrons in the d-orbital) results in shifting up of antibonding states through the Fermi level and lower occupancy of anti-bonding states, leading to the stronger interaction between the adsorbate and the catalyst surface. The *d*-band center of Pd cluster is estimated to be –1.82, –1.81, –1.78, –1.75, and –1.73 eV for Pd@UiO-66-2OH, Pd@UiO-66-2OH(Hf), Pd@UiO-66-NH_2, Pd@UiO-66-OMe, and Pd@UiO-66, respectively. It is well known that, when the *d*-band center gets closer to zero (Fermi level), the interaction between the reactant and the surface will be stronger, accordingly larger adsorption energy. Therefore, according to the *d*-band center data above, the adsorption strength sequence of substrates on Pd_{28}@UiO-66-X should be Pd@UiO-66-2OH < Pd@UiO-66-2OH(Hf) < Pd@UiO-66-NH_2 < Pd@UiO-66-OMe < Pd@UiO-66 (**Figure 4**), which is exactly reverse to that of catalytic activity. Given that appropriate adsorptive strength between substrate and active center/catalyst is favorable, and too strong strength is detrimental to catalytic reactions, based on the Sabatier principle,[12] these adsorption energy results well explain and should account for the order of experimental activity (Figure 4).

Encouraged by the above theoretical and characterization elucidations, the general applicability of the optimized Pd@UiO-66-2OH catalyst for selective hydrogenation of diverse benzoic acid derivatives has been further investigated (Table S2, Supporting Information). To our delight, all para-substituted benzoic acids with both electron-drawing and -donating groups (–Cl, –Br, $–CH_3$) have shown excellent conversion and selectivity (entry 1–3). The hydrogenation of phenyl acetic acid, a homologous compound of benzoic acid, also gives complete conversion (entry 4). Moreover, the benzoic acid derivatives, methyl benzoate and benzamide afford very high conversions of 99% and 95%, respectively (entry 5–6). Their similarly high activities well illuminate the general applicability of Pd@UiO-66-2OH, tolerating various benzoic acid derivatives.

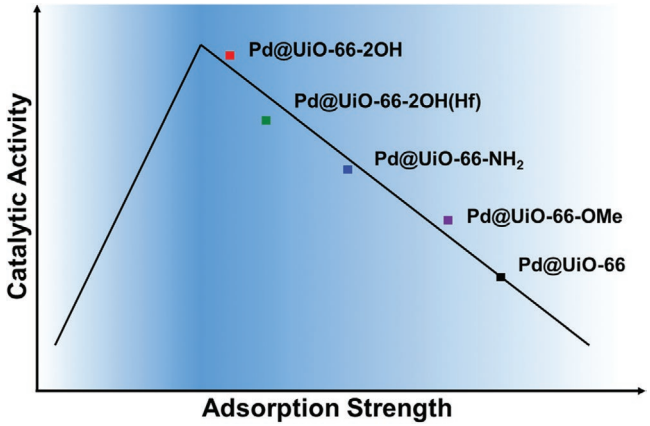

Figure 4. Schematic plot guiding the relationship between adsorption strength and catalytic activity.

In summary, isoreticular UiO-66-X with various linker groups and altered M-oxo clusters have been synthesized. The ultrafine Pd NPs are incorporated into these MOF pores, which create modulated chemical microenvironment for Pd sites based on the MOF pore wall engineering. The selective hydrogenation of benzoic acid to CCA, a vital process in petroleum industry, has been selected to investigate the catalytic performance of Pd@UiO-66-X. Remarkably, their activities are distinctly different, among which Pd@UiO-66-2OH is not only 14 times higher than that of Pd@UiO-66 but also exhibits excellent conversions toward diverse benzoic acid derivatives. The different Pd electronic states in Pd@UiO-66-X, attributed to the differentiated charge transfer interactions between Pd and the isoreticular MOFs, should be responsible for the above results. Furthermore, the calculated *d*-band center results reveal that the discriminative adsorption energy of these Pd@UiO-66-X catalysts also accounts for their distinct activities. As far as we know, this is the first work tailoring electronic state and adsorption energy of metal NPs by means of linker group change and metal substitution in isoreticular MOF hosts. This work provides significant insight in the design of heterogeneous catalysts and will open up an avenue to the rational control of chemical microenvironment surrounding active sites for optimizing catalytic performance. We believe this microenvironment effect on catalysis would be extendable to other metal/MOF catalytic systems, and even other heterogeneous catalytic systems.

Supporting Information

Supporting Information is available from the Wiley Online Library or from the author.

Acknowledgements

D.C., W.Y., and L.J. contributed equally to this work. This work was supported by the National Natural Science Foundation of China (21725101, 21871244, 21673213, and 21521001), the China Postdoctoral Science Foundation (2019M660151, 2019TQ0298), and Fujian Institute of Innovation (CAS). The authors gratefully thank all reviewers for their insightful comments and valuable suggestions, Dr. X. Liu at University of Science and Technology of China for discussions.

Conflict of Interest

The authors declare no conflict of interest.

Keywords

adsorption energy, electron transfer, metal nanoparticles, metal–organic frameworks, microenvironment regulation

Received: January 3, 2020
Revised: April 29, 2020
Published online:

[1] a) M. Haruta, *Nature* **2005**, *437*, 1098; b) R. M. Crooks, M. Zhao, L. Sun, V. Chechik, L. K. Yeung, *Acc. Chem. Res.* **2001**, *34*, 181; c) L. Liu, A. Corma, *Chem. Rev.* **2018**, *118*, 4981; d) B. Wu, N. Zheng, *Nano Today* **2013**, *8*, 168.

[2] a) R. J. White, R. Luque, V. L. Budarin, J. H. Clark, D. J. Macquarrie, *Chem. Soc. Rev.* **2009**, *38*, 481; b) Q.-L. Zhu, Q. Xu, *Chem* **2016**, *1*, 220; c) M. Zhao, K. Yuan, Y. Wang, G. Li, J. Guo, L. Gu, W. Hu, H. Zhao, Z. Tang, *Nature* **2016**, *539*, 76; d) P. Liu, R. Qin, G. Fu, N. Zheng, *J. Am. Chem. Soc.* **2017**, *139*, 2122.

[3] a) H.-C. Zhou, J. R. Long, O. M. Yaghi, *Chem. Rev.* **2012**, *112*, 673; b) H.-C. Zhou, S. Kitagawa, *Chem. Soc. Rev.* **2014**, *43*, 5415; c) L. Jiao, Y. Wang, H.-L. Jiang, Q. Xu, *Adv. Mater.* **2018**, *30*, 1703663; d) B. Li, H.-M. Wen, Y. Cui, W. Zhou, G. Qian, B. Chen, *Adv. Mater.* **2016**, *28*, 8819; e) T. Islamoglu, S. Goswami, Z Li, A. J. Howarth, O. K. Farha, J. T. Hupp, *Acc. Chem. Res.* **2017**, *50*, 805; f) C. Wang, B. An, W. Lin, *ACS Catal.* **2019**, *9*, 130. g) B. Pattengale, S. Yang, J. Ludwig, Z. Huang, X. Zhang, J. Huang, *J. Am. Chem. Soc.* **2016**, *138*, 8072; h) G. Li, S. Zhao, Y. Zhang, Z. Tang, *Adv. Mater.* **2018**, *30*, 1800702; i) D. Zhang, Y. Zhu, L. Liu, X. Ying, C.-E. Hsiung, R. Sougrat, K. Li, Y. Han, *Science* **2018**, *359*, 675; j) X. Zhao, Y. Wang, D.-S. Li, X. Bu, P. Feng, *Adv. Mater.* **2018**, *30*, 1705189; k) M. Zhao, S. Ou, C.-D. Wu, *Acc. Chem. Res.* **2014**, *47*, 1199; l) K. J. Lee, J. H. Lee, S. Jeoung, H. R. Moon, *Acc. Chem. Res.* **2017**, *50*, 2684; m) T. Kundu, M. Wahiduzzaman, B. B. Shah, G. Maurin, D. Zhao, *Angew. Chem., Int. Ed.* **2019**, *58*, 8073; n) G. Cai, M. Ding, Q. Wu, H.-L. Jiang, *Natl. Sci. Rev.* **2020**, *7*, 37.

[4] a) Q. Yang, Q. Xu, H.-L. Jiang, *Chem. Soc. Rev.* **2017**, *46*, 4774; b) G. Lu, S. Li, Z. Guo, O. K. Farha, B. G. Hauser, X. Qi, Yi Wang, X. Wang, S. Han, X. Liu, J. S. DuChene, H. Zhang, Q. Zhang, X. Chen, J. Ma, S. C. J. Loo, W. D. Wei, Y. Yang, J. T. Hupp, F. Huo, *Nat. Chem.* **2012**, *4*, 310; c) J. Hermannsdörfer, M. Friedrich, N. Miyajima, R. Q. Albuquerque, S. Kümmel, R. Kempe, *Angew. Chem., Int. Ed.* **2012**, *51*, 11473; d) P. Hu, J. Zhuang, L.-Y. Chou, H. K. Lee, X. Ling, Y.-C. Chuang, C.-K. Tsung, *J. Am. Chem. Soc.* **2014**, *136*, 10561; e) Y. Huang, S. Liu, Z. Lin, W. Li, X. Li, R. Cao, *J. Catal.* **2012**, *292*, 111; f) D. Jiang, G. Fang, Y. Tong, X. Wu, Y. Wang, D. Hong, W. Leng, Z. Liang, P. Tu, L. Liu, K. Xu, J. Ni, X. Li, *ACS Catal.* **2018**, *8*, 11973.

[5] a) X. Li, T. W. Goh, L. Li, C. Xiao, Z. Guo, Xiao C. Zeng, W. Huang, *ACS Catal.* **2016**, *6*, 3461; b) K. M. Choi, K. Na, G. A. Somorjai, O. M. Yaghi, *J. Am. Chem. Soc.* **2015**, *137*, 7810; c) H. Liu, L. Chang, L. Chen, Y. Li, *ChemCatChem* **2016**, *8*, 946; d) H. Kobayashi, J. M. Taylor, Y. Mitsuka, N. Ogiwara, T. Yamamoto, T. Toriyama, S. Matsumura, H. Kitagawa, *Chem. Sci.* **2019**, *10*, 3289; e) S. Yoshimaru, M. Sadakiyo, A. Staykov, K. Katoc, M. Yamauchi, *Chem. Commun.* **2017**, *53*, 6720; f) Y. Tong, G. Xue, H. Wang, M. Liu, J. Wang, C. Hao, X. Zhang, D. Wang, X. Shi, W. Liu, G. Li, Z. Tang, *Nanoscale* **2018**, *10*, 16425.

[6] a) J. H. Cavka, S. Jakobsen, U. Olsbye, N. Guillou, C. Lamberti, S. Bordiga, K. P. Lillerud, *J. Am. Chem. Soc.* **2008**, *130*, 13850; b) S. Biswas, P. Van der Voort, *Eur. J. Inorg. Chem.* **2013**, *2013*, 2154; c) H. Wu, Y. S. Chua, V. Krungleviciute, M. Tyagi, P. Chen, T. Yildirim, W. Zhou, *J. Am. Chem. Soc.* **2013**, *135*, 10525.

[7] a) A. Aijaz, A. Karkamkar, Y. J. Choi, N. Tsumori, E. Rönnebro, T. Autrey, H. Shioyama, Q. Xu, *J. Am. Chem. Soc.* **2012**, *134*, 13926; b) Y.-Z. Chen, Y.-X. Zhou, H. Wang, J. Lu, T. Uchida, Q. Xu, S.-H. Yu, H.-L. Jiang, *ACS Catal.* **2015**, *5*, 2062.

[8] a) H. Shinkai, K. Toi, I. Kumashiro, Y. Seto, M. Fukuma, K. Dan, S. Toyoshima, *J. Med. Chem.* **1988**, *31*, 2092; b) X. Ren, M. Guo, H. Li, C. Li, L. Yu, J. Liu, Q. Yang, *Angew. Chem., Int. Ed.* **2019**, *58*, 14483; c) X. Xu, M. Tang, M. Li, H. Li, Y. Wang, *ACS Catal.* **2014**, *4*, 3132; d) M. Tang, S. Mao, M. Li, Z. Wie, F. Xu, H. Li, Y. Wang, *ACS Catal.* **2015**, *5*, 3100.

[9] a) G. Kresse, J. Hafner, *Phys. Rev. B* **1993**, *47*, 558; b) G. Kresse, J. Furthermüller, *Phys. Rev. B* **1996**, *54*, 11169; c) B. Hammer, J. K. Nørskov, *Adv. Catal.* **2000**, *45*, 71.

[10] M. Skotak, Z. Karpiński, W. Juszczyk, J. Pielaszek, L. Kępiński, D. V. Kazachkin, V. I. Kovalchuk, J. L. d'Itri, *J. Catal.* **2004**, *227*, 11.

[11] a) H. Xu, D. Cheng, D. Cao, X. C. Zeng, *Nat. Catal.* **2018**, *1*, 339; b) A. Vojvodic, J. K. Nørskov, F. Abild-Pedersen, *Top. Catal.* **2014**, *57*, 25.

[12] J. Cheng, P. Hu, *J. Am. Chem. Soc.* **2008**, *130*, 10868.

